RSC Advances

PAPER

View Article Online
View Journal | View Issue

Cite this: *RSC Adv.*, 2018, **8**, 34860

Specific colorimetric detection of Fe^{3+} ions in aqueous solution by squaraine-based chemosensor†

Xiaoqian Liu, *[a] Na Li,[a] Min-Min Xu,[b] Jianhao Wang,[a] Chunhui Jiang,[c] Guoqiang Song*[a] and Yong Wang *[b]

Received 3rd September 2018
Accepted 2nd October 2018

DOI: 10.1039/c8ra07345g

rsc.li/rsc-advances

A new squaraine based chemosensor **TSQ** was developed for colorimetric detection of Fe^{3+} ions. A thymine moiety in **TSQ** was constructed to act as an ion acceptor. The sensor displayed an instant colorimetric response specific to Fe^{3+} over the other metal ions in 20% AcOH–H_2O solution. The limit of detection was much lower than that of the environmental protection agency guideline (5.37 μM) in drinking water. A 1 : 1 binding between **TSQ** and Fe^{3+} ion was evidenced by Job's plot measurement, ESI-MS and Fourier transform infrared (IR) measurements. Moreover, the proposed sensing mechanism of the receptor towards Fe^{3+} was strongly supported by DFT calculation. Finally, the sensor has proven to be suitable in real sample applications.

1 Introduction

For the past years, the development of highly sensitive and selective chemosensors has been attracting great interests for detecting heavy metals due to their importance in environmental, biology and chemistry domains.[1–10] Iron, the third most abundant element on the earth, is not only the ubiquitous element in the environment, but also an essential element in living cells. It plays crucial roles in functional biological processes, such as cellular metabolism, enzymatic reactions, oxygen transport and gene expression.[11–16] Both deficiency and excess can cause a series of diseases.[17] Current qualitative and quantitative determination methods for Fe^{3+} ions include atomic absorption spectroscopy, inductively coupled plasma-atomic emission spectroscopy, mass spectrometry, electrochemical and fluorescence spectroscopic analysis.[18–22] These methods suffer either from the sophisticated nature and high cost of instruments, or from tedious sample preparation procedures.[23,24] It is imperative to develop simple, highly sensitive and selective chemosensors for Fe^{3+} detection. To date, a few chemosensors have been developed based on functioned nanoparticles or conjugated organic chromophores.[25–32] However, few of them can be used as practical probes limited by their low sensitivity and selectivity, as well as incompatibility with aqueous environments.[33–37] For example, Hg^{2+}, Zn^{2+} as well as Cu^{2+}, which exhibit many properties similar to those of Fe^{3+}, could interfere the Fe^{3+} detection.[38,39] Also it is noted that not many chemosensors with long absorption wavelength have been reported so far. Hence, to develop efficient colorimetric sensing materials still remains a big challenge.

Squaraines are versatile organic dyes which have shown intense absorption in near infrared region and have been widely applied in the optoelectronics fields such as light emitting diodes, field-effect transistors and chemosensors.[40–46] Taken advantages of their unique properties, squaraine-based ion sensors can be constructed by a combination of squaraine chromophores with ligands. The intramolecular charge transfer will be occurred once metal ions have interacted with designed ion receptor. This could result in a rich modulation of color changes.

Thymine is one of the four nucleobases to perform base paring with adenine in constructing double helix DNA. It has proven to be one of the most effective ligands binding to the metal ions especially for mercury ion.[47] Therefore, we introduced a thymine group into the squaraine chromophore, leading to a new thymine-squaraine based chemosensor. To our surprise, the resulting chemosensor can specifically detect Fe^{3+} over the other metal ions by color change in aqueous solution. The complexation to Fe^{3+} and sensing mechanism were further investigated by Job's plot measurement, UV-vis titration, ESI-MS spectrometry analysis, IR analysis and theoretical calculation. The improvement in the color response, rapid accurate recognition of Fe^{3+} and low detection limit make this approach very promising for Fe^{3+} detection.

[a]*School of Pharmaceutical Engineering and Life Science, Changzhou University, 213164, Jiangsu, China. E-mail: chmliux@cczu.edu.sg; sgq@cczu.edu.cn*

[b]*College of Chemistry, Chemical Engineering and Materials Science, Soochow University, Suzhou 215123, PR China. E-mail: yowang@suda.edu.cn*

[c]*School of Environmental and Chemical Engineering, Jiangsu University of Science and Technology, 2 Mengxi Road, Zhenjiang, Jiangsu, 212003, China*

† Electronic supplementary information (ESI) available. See DOI: 10.1039/c8ra07345g

2 Experimental section

2.1 Reagents and apparatus

All the reagents related to the starting materials for synthesizing **TSQ** in Scheme 1 and the inorganic salts together with buffer used in the properties study of **TSQ** were obtained from commercial available sources in analytical grade without purification. ^{1}H NMR (400 MHz) and ^{13}C NMR (400 MHz) spectra were recorded on a Bruker AV-400 spectrometer using a deuterated solvent as the lock and TMS as an internal reference. Mass spectrometry analysis was performed on a Q exactive mass spectrometer (Thermo Fisher Scientific, USA). Absorption spectra were measured on Molecular Device Spectrometer 5 (Molecular Devices Corporation, USA).

2.2 Synthesis of TSQ

The synthetic pathway for **TSQ** was illustrated in Scheme 1. A mixture of A1 (1.351 g, 1.8 mmol) and A2 (0.375 g, 1.8 mmol) were dissolved in *N*,*N*-dimethylformamide (20 mL) together with amide coupling reagents of *N*,*N*-diisopropylethylamine (0.225 g, 3.6 mmol), 1-(3-dimethylaminopropyl)-3-ethylcarbodiimide hydrochloride (0.342 g, 1.98 mmol) and 1-hydroxybenzotriazole (0.243 g, 1.8 mmol). The mixture was stirred for 4 h at room temperature. It was monitored by thin layer chromatography and purified by column chromatography using DCM : MeOH = 30 : 1 as eluents. The final compound **TSQ** was obtained as dark solid in the yield of 45.2%. The structure was confirmed by NMR and mass spectrometric analysis (Fig. S1 and S2†). ^{1}H NMR (400 MHz, $CDCl_3$) δ: 10.41 (s, 1H), 7.99 (s, 2H), 7.89–7.84 (m, 2H), 7.37–7.30 (m, 2H), 7.19–7.16 (m, 2H), 7.04–7.02 (m, 2H), 6.94–6.92 (d, J = 7.9 Hz), 5.97–5.92 (m, 2H), 4.37 (s, 1H), 4.09–4.07 (d, J = 6.6 Hz, 2H), 3.89 (s, 1H), 3.58 (s, 2H), 3.50 (m, 4H), 1.76–1.70 (m, 16H), 1.35–1.22 (m, 15H), 0.87–0.82 (m, 3H). ^{13}C NMR (100 MHz, $CDCl_3$) δ: 181.28, 177.93, 171.20, 168.85, 168.02, 167.93, 164.66, 151.62, 145.46, 142.42, 141.66, 141.09, 129.93, 129.89, 128.54, 128.05, 127.98, 124.43, 122.44, 121.44, 111.07, 109.66, 108.75, 87.37, 86.77, 50.70, 49.72, 48.68, 43.77, 40.29, 38.72, 31.73, 29.70, 29.37, 29.33, 29.17 27.07, 27.00, 26.80, 22.59, 14.13, 14.09, 12.30,12.13 ppm. ESI-MS calculated for **TSQ** 788.4261, found 789.5288.

2.3 UV-vis spectroscopy

A stock solution of **TSQ** was prepared 10 mM in DMSO. Further dilutions were made to prepare 100 μM of **TSQ** by adding different types of solutions. 11 different metal salts were prepared 10 mM in distilled water and diluted further accordingly. After mixing **TSQ** and metal ion solutions, the absorption measurements were made in 96 well plates on Molecular Device Spectrometer 5 (Molecular Devices Corporation, USA) at the wavelength range of 350 nm to 750 nm.

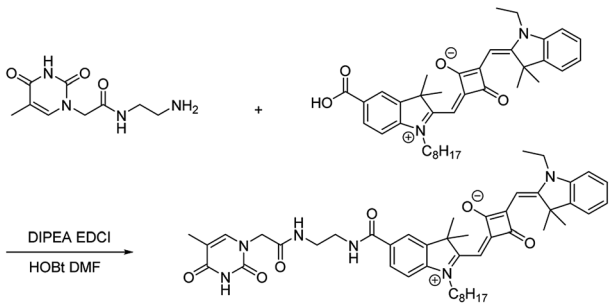

Scheme 1 Synthetic pathway for chemosensor TSQ.

2.4 Job's plot measurements

The stock solution of sensor **TSQ** (10 mM) in DMSO and $FeCl_3$ (10 mM) in distilled water were prepared, respectively. When the mole fraction of Fe^{3+} was equal to 0.1, the sensor **TSQ** solution (1.8 μL) and $FeCl_3$ solution (0.2 μL) were added to each 20% AcOH solution to make a total volume of 200 μL. After stirring for a few seconds, UV-vis spectra were recorded at room temperature. When the mole fraction gradually increased to 1.0, **TSQ** volume decreased by 0.2 μL and Fe^{3+} volume increased by 0.2 μL, respectively. The absorption spectra were recorded at absorption maximum wavelength. The plots were drawn by plotting $A_0/(A_0 - A)$ *vs.* $1/[Fe^{3+}]$, where A_0 equaled to absorption intensity of **TSQ** without Fe^{3+}, A was corresponding to the absorption intensity of **TSQ** with different concentrations of Fe^{3+}.

2.5 Competition tests

2 μL of Na^+, K^+, Li^+, Ag^+, Zn^{2+}, Hg^{2+}, Cd^{2+}, Fe^{2+}, Co^{2+}, Ca^{2+} ion solutions (10 mM) were extracted individually and mixed with 2 μL Fe^{3+} (2 mM), 2 μL **TSQ** (10 mM) and filled up with 20% AcOH–H_2O solution to total volume of 200 μL. After stirring the solutions for a few seconds, UV-vis spectra were recorded at room temperature.

3 Results and discussion

3.1 Spectral properties of TSQ

The absorption properties of **TSQ** were investigated in different aqueous solutions, *i.e.* distilled pure water, phosphate buffer (PBS buffer, pH = 7.4), borate buffer (pH = 6.8) and acetic acid. The results were recorded as shown in Fig. 1a. Two broad absorption peaks of **TSQ** were observed at 605 nm and 660 nm once the water was present (distilled pure water, phosphate buffer and borate buffer). The sensor has shown a cyan color in the solution. Only one strong and symmetric peak was observed at 635 nm which has been shown as blue color in the presence of pure acetic acid. It is well known that squaraines have great tendency to aggregate in a different pattern which corresponding to the interesting spectroscopic response. A blue shifted absorption and broaden absorption peaks will be observed as in H-aggregation (paralleled oriented arrangement) and red shifted absorption and sharp absorption peaks will be shown as in J-aggregation (head to tail fashion). In this case, it is assumed that the different extent and H-aggregation occur in the presence of water by **TSQ**. To further validate the water induced aggregation effect, the different percentage of water was added into acetic acid to form acetic acid solution. As shown in Fig. 1b, as the percentage of water in acetic acid increased, the absorption performances were almost preserved even in the presence of 60% H_2O in acetic acid solution. With further increased water percentage to 80%, the intensity of new weak band at 650 nm

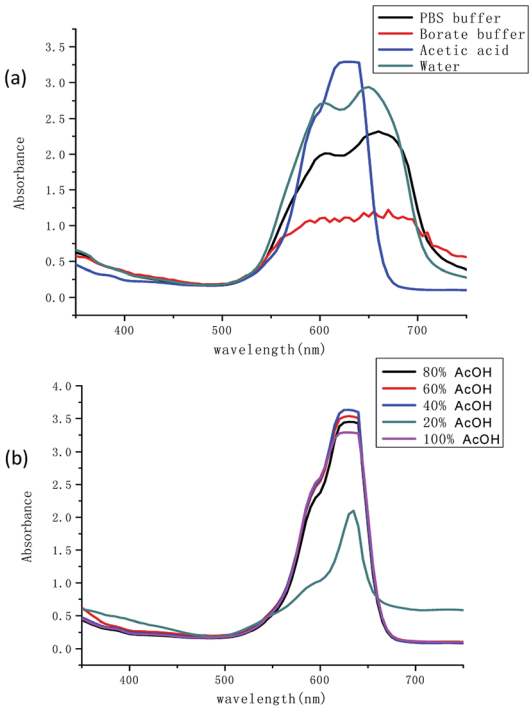

Fig. 1 (a) UV-vis spectra of **TSQ** (100 μM) in different aqueous solutions and (b) in the mixture of AcOH–H_2O.

concomitantly increased (blue shift) which was consistent with results in Fig. 1a. For both PBS buffer (pH = 7.4) and borate buffer (pH = 6.8), the pH of the solvent system has no significant influence on the absorption spectrum.

3.2 Colorimetric sensing for Fe^{3+}

Preliminary results have shown that **TSQ** could possess good absorption properties in acetic acid, which were selected for identifying the metal ions in the following experiments.

Colorimetric responses to various metal ions including Na^+, K^+, Li^+, Ag^+, Zn^{2+}, Hg^{2+}, Cd^{2+}, Fe^{2+}, Co^{2+}, Ca^{2+}, Fe^{3+} were investigated. It has shown in Fig. 2a that in 20% AcOH–H_2O solution of 100 μM **TSQ**, the color change was dramatic and specific to Fe^{3+}, while addition of other metal ions did not show any significant change. The Fe^{3+} induced a spontaneous color change from blue to green, which could be easily detected by the naked eyes. In the corresponding UV-vis spectrum, the intensity of strong absorption at 635 nm was decreased after the addition of Fe^{3+}.

The solvent effects on detection of Fe^{3+} for **TSQ** in AcOH–H_2O solution were further evaluated (Fig. 3). By varying the portion of AcOH in the distilled water, the decreased absorption change of **TSQ** only can be observed in 20% AcOH–H_2O solution. There were no similar observations in other solutions, which indicating that **TSQ** was a highly sensitive and selective colorimetric sensor for Fe^{3+} ions.

3.3 Time-resolved colorimetric study

For the purpose of exploring the relationship between absorption intensity and response time, a dynamic study of **TSQ** in the detection of Fe^{3+} was monitored. The green color of **TSQ** was

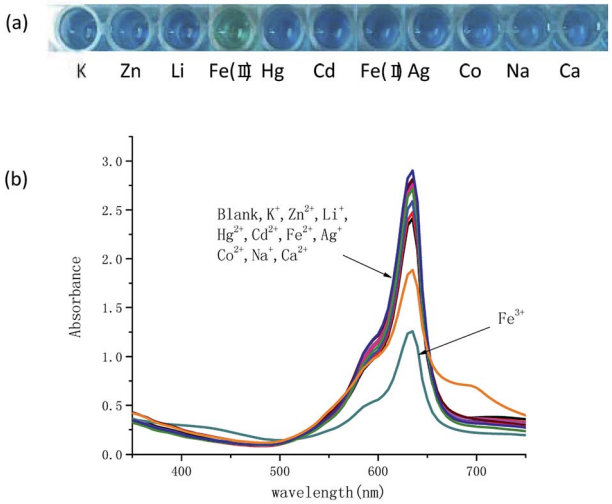

Fig. 2 (a) Visualization and (b) absorption spectra for **TSQ** solution (100 μM) with/without addition of different metal ions (100 μM) in 20% AcOH–H_2O.

kept even after 4 hours which clearly indicated that the detection for Fe^{3+} was instant and the complexation reaction was stable (Fig. 4).

3.4 Binding constant K_a and limit of detection (LOD) for Fe^{3+}

To get insight into the binding mode between **TSQ** and Fe^{3+}, the UV-vis absorption spectra of 100 μM **TSQ** in 20% AcOH–H_2O solution were recorded during the titration of various concentrations of Fe^{3+}. The binding constant (K_a) was estimated using a Benesi–Hildebrand plot, which was calculated by absorption changes of consequent titration ($A_0/A_0 - A$) against $1/[Fe^{3+}]$. The magnitude of Ka was calculated from the intercept and slope of the straight line, and the estimated value is about $9.6 \times 10^5\ M^{-1}$ (Fig. 5). More importantly, the absorption change of **TSQ** corresponded to the concentration of Fe^{3+} in a linear manner in the range of 1–100 μM. The high sensitivity of this sensor in 20% AcOH–H_2O solution allowed detection limit reaching to be 1 μM. The detection limit of Fe^{3+} was much lower than the EPA guidelines for drinking water of 5.37 μM.[48] The sensing ability of

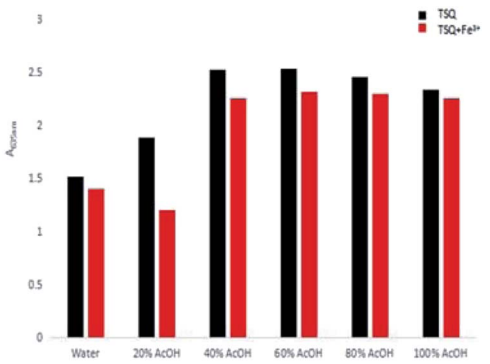

Fig. 3 Bar chart showing the absorption changes of **TSQ** (100 μM) in the different AcOH–H_2O solution with adding 100 μM Fe^{3+} (red bar) or without Fe^{3+} (black).

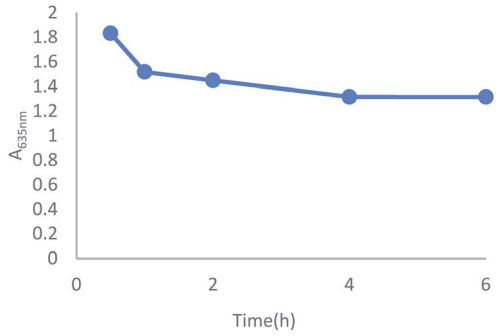

Fig. 4 Dynamic study on the absorption change by mixing **TSQ** (100 μM) and Fe^{3+} (100 μM) in 20% AcOH–H_2O solution.

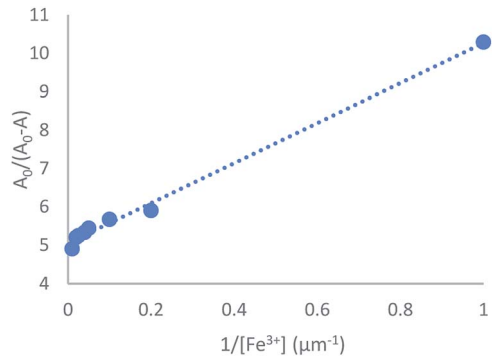

Fig. 5 Benesi–Hildebrand plot analysis of the absorption changes for the complexation between **TSQ** and Fe^{3+}, $R^2 = 0.9947$.

TSQ towards Fe^{3+} was also compared to those for coumarin and rhodamine derivatives, which considering as other two types of promising near infrared colorimetric sensing probes. The LOD of present probe **TSQ** is superior to those of coumarin derivative[49,50] and rhodamine based chemosensors[31] (Table S1†).

3.5 Complexation mechanism of TSQ–Fe^{3+}

Job's plot measurement was carried out to explore the binding ratio of **TSQ** and Fe^{3+} (Fig. 6). The plots were done by recording the absorption intensity *A* against [Fe^{3+}]/[Fe^{3+}]+[**TSQ**]. The results revealed that the **TSQ** probe bind with Fe^{3+} in 1 : 1 stoichiometry, which was further confirmed by ESI-MS data. A solution containing **TSQ** and 1 equiv. of $FeCl_3$ has shown a strong peak at *m*/*z* 905.5341, assigned to [**TSQ** + Fe^{3+} + CH_3-COOH + H^+] ion (Fig. S3†). IR spectra can provide valuable information on the complexation. To gain additional insight into the Fe^{3+} binding properties, the FT-IR spectra of **TSQ** and **TSQ**–Fe^{3+} complex were measured (Fig. 7). The shift of the carbonyl absorption band indicated the change of structure. The characteristic amide carbonyl (C=O) stretching vibrations at 1685 cm^{-1} shifted to 1608 cm^{-1} in the presence of Fe^{3+}, while the characteristic carbonyl (C=O) stretching frequencies in thymine moiety appeared at 1584 cm^{-1} instead of 1596 cm^{-1} in the complex of **TSQ**–Fe^{3+}. In addition, a new broad peak was generated at 3400 cm^{-1} which corresponding to the N–H vibration. All these results strongly indicate the amide carbonyl O atom (C=O) and the carbonyl O atom in thymine moiety were

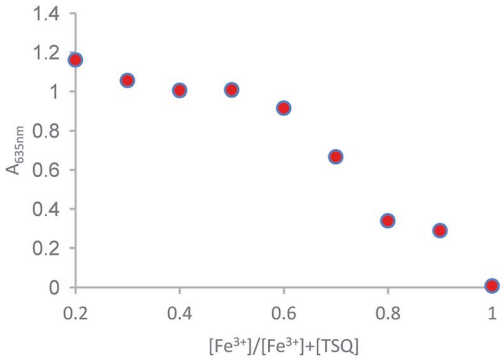

Fig. 6 Job's plot for the complexation of **TSQ** with Fe^{3+} in AcOH–H_2O (2 : 8, v/v) solution.

involved in the recognition of Fe^{3+}. The density functional theory (DFT) study was further in proceed to get insight into details of **TSQ**–Fe^{3+} complexation. All calculations were carried out with the Gaussian 09 package.[51] The density functional theory (DFT) hybrid model with the B3LYP was used for the gas-phase geometry optimizations, Lanl2dz basis set with effective core potential (ECP) for Fe, and the 6-31G(d) basis set was used for all remaining atoms. Based on the calculations, the favourability binding mode between **TSQ** (a) and its Fe^{3+} complex (b) was depicted in Fig. 8. It is favourable for the thymine moiety, which was vertical to the planar of asymmetrical squaraine dyes. And the Fe^{3+} ion was tended to bind with one carbonyl group in thymine and another carbonyl group on the oxygen atom of amide bond. All conformations were calculated at the same level to confirm their stability (no imaginary frequencies).

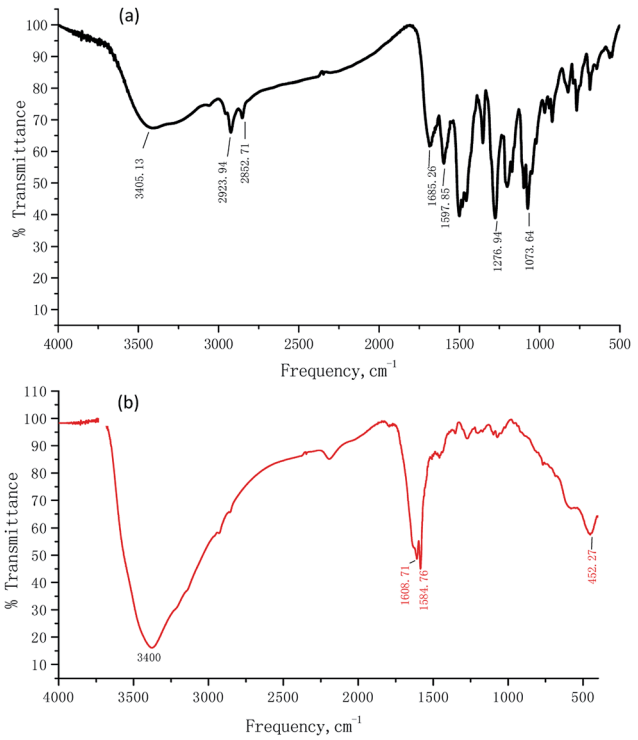

Fig. 7 The IR spectra of **TSQ** (Black line) and **TSQ**–Fe^{3+} (Red line).

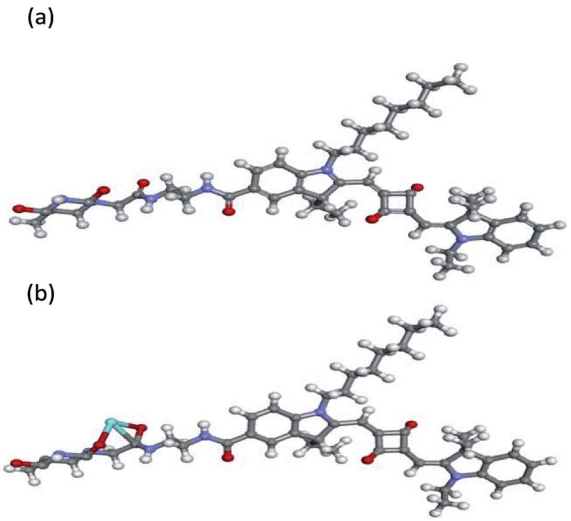

Fig. 8 The geometry-optimized structures of **TSQ** (a) and its Fe^{3+} complex (b) at the SMD (H_2O)-TD-PBE0/TZVP + LANL2DZ level.

3.6 Ions interference effects on the TSQ towards Fe^{3+}

Counterion effects on the sensitive colorimetric sensor **TSQ** for Fe^{3+} have also been investigated. The results have shown that the anions with weak coordination abilities towards Fe^{3+} such as Cl^-, SO_4^{2-}, SO_3^{2-}, NO^{3-}, CO_3^{2-} had no predominant effect on the absorption change (Fig. 9). In addition, the colorimetric responses towards other environmentally relevant metal ions were recorded as well. Upon addition of 5 equiv. Na^+, K^+, Li^+, Ag^+, Zn^{2+}, Hg^{2+}, Cd^{2+}, Fe^{2+}, Co^{2+}, Ca^{2+} in **TSQ**–Fe^{3+} complex solution, no apparent absorption changes were observed, indicating that extra amount of other cations have no significant interference to the response of **TSQ** towards Fe^{3+} (Fig. 10).

3.7 Reversible study of TSQ–Fe^{3+} complex towards EDTA

In order to test if the proposed **TSQ**–Fe^{3+} complex could be reversed, EDTA as a strong chelator was added to the solution containing of 1 equiv. **TSQ** and 1 equiv. Fe^{3+}. As seen in Fig. 11, the addition of 1 equiv. EDTA restored the absorption signal of **TSQ** to its original level. Additional 1 equiv. Fe^{3+} was added in again to make another round of detection by colorimetric change from blue to green (Fig. S4†). All these results show that the process of titrating sensor **TSQ** with Fe^{3+} is reversible and that sensor **TSQ** could be used as an on-off-on switch chemosensor.

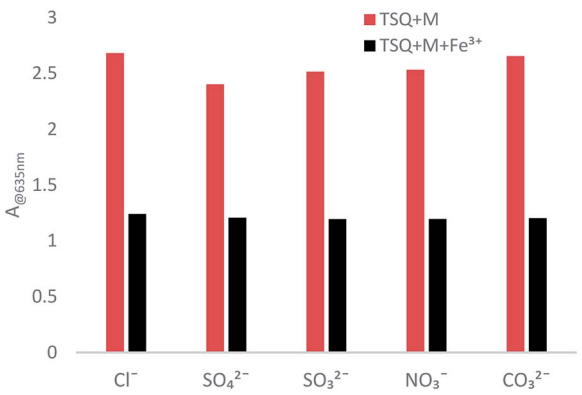

Fig. 9 Absorption changes of **TSQ**–Fe^{3+} in the presence of various test anions in AcOH–H_2O (2 : 8, v/v).

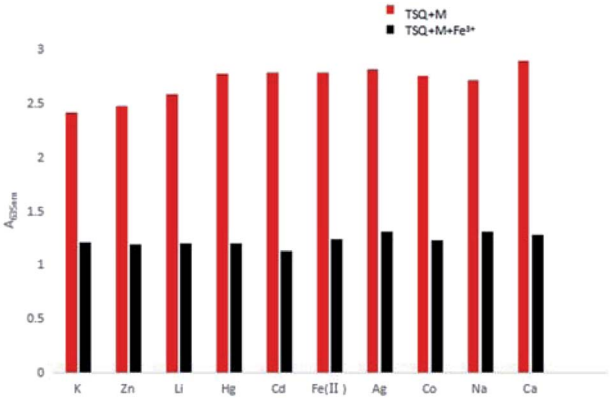

Fig. 10 Absorption changes of **TSQ**–Fe^{3+} in the presence of various test cations in AcOH–H_2O (2 : 8, v/v).

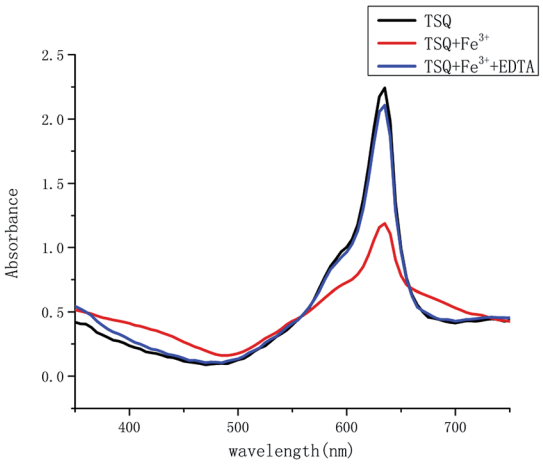

Fig. 11 Absorption spectra of **TSQ** (100 μM) + Fe^{3+} (100 μM) upon the addition of EDTA (1 equiv.) in AcOH–H_2O (2 : 8, v/v).

3.8 Preliminary analytical applications

In order to examine the capability of the proposed chemosensor in environmental samples, **TSQ** was applied to the determination of the Fe^{3+} in waste water from an electroplating factory. As shown in Table 1, the initial Fe^{3+} concentrations were measured by the atomic absorption spectrometry (AAS) method and three levels of standard concentrations of Fe^{3+} were added into real

Table 1 Determination of Fe^{3+} ion in waste water samples with **TSQ**

Sample	AAS (μM)	Added (mM)	Found (mM)	Recovery (%)
Waste water 1	2.08	1.20	1.22	101.2
Waste water 2	3.78	2.31	2.38	103.3
Waste water 3	6.02	3.62	3.58	99.0

samples. By applying our **TSQ** test, the content of Fe^{3+} in waste water was in good agreement with that added amount by a relative error in less than 5%. Therefore, the present **TSQ** was initially proven to be well used in the determination of Fe^{3+} in real samples.

4 Conclusions

In summary, we have successfully constructed a thymine-squaraine based colorimetric chemosensor for Fe^{3+} detection in aqueous solution. It has shown an excellent selectivity for Fe^{3+} over the other cations (blue to green). The limited of detection (1 μM) was determined lower than the EPA guidelines for drinking water of 5.37 μM and no other ion interferences have shown significant effects on the Fe^{3+} detection. Further study of mechanism by Job's plot measurement, ESI-MS indicated that 1 : 1 complex was formed between **TSQ** and Fe^{3+}. IR spectrum and DFT calculation further revealed the detailed binding mode of **TSQ**–Fe^{3+} complex in the way of binding on the amide carbonyl O atom (C═O) and the carbonyl O atom on thymine moiety towards Fe^{3+}. Reversible study and preliminary analytical application study have shown strong potent of **TSQ** as a good chemosensor to Fe^{3+} in real sample applications. Considering that the developed thymine-squaraine based chemosensor **TSQ** was quite effective and selective, we expect that it will potentially serve as colorimetric probe for more Fe^{3+}-related environmental studies.

Conflicts of interest

There are no conflicts to declare.

Acknowledgements

This work were financially supported by research fund for Jiangsu specially appointed professor (SCZ1505200002 and SCZ1606600001), foundation of Jiangsu High Education Committee for natural science research projects (18KJB150005) and Postdoctoral Science Foundation in Jiangsu Province (2018K275C).

Notes and references

1 J. Yin, Y. Hu and J. Yoon, *Chem. Soc. Rev.*, 2015, **44**, 4619–4644.
2 X. H. Li, X. H. Gao, W. Shi and H. M. Ma, *Chem. Rev.*, 2014, **114**, 590–659.
3 J. Sun, B. Ye, G. Xia, X. Zhao and H. Wang, *Sens. Actuators, B*, 2016, **233**, 76–82.
4 X. Zhou, S. Lee, Z. Xu and J. Yoon, *Chem. Rev.*, 2015, **115**, 7944–8000.
5 X. X. Hu, X. L. Zheng, X. X. Fan, Y. T. Su, X. Q. Zhan and H. Zheng, *Sens. Actuators, B*, 2016, **227**, 191–197.
6 K. P. Carter, A. M. Young and A. E. Palmer, *Chem. Rev.*, 2014, **114**, 4564–4601.
7 O. Anderson, *Chem. Rev.*, 1999, **99**, 2683–2710.
8 W. Qin, W. Dou, V. Leen, W. Dehan, M. W. Auweraer and N. Boens, *RSC Adv.*, 2016, **6**, 7806–7816.
9 S. Sinha, T. Mukherjee, J. Mathew, S. K. Mukhopadhyay and S. Ghosh, *Anal. Chim. Acta*, 2014, **822**, 60–68.
10 C. Li, J. Qin, G. Wang, B. Wang, A. Fu and Z. Zhang, *Inorg. Chim. Acta*, 2015, **430**, 91–95.
11 H. Matthias, U. M. Martina, G. Bruno and C. Clara, *Cell*, 2010, **142**, 24–38.
12 S. K. Danuta and R. R. Des, *Pharmacol. Rev.*, 2015, **57**, 547–583.
13 R. Meneghini, *Free Radical Biol. Med.*, 1997, **23**, 783–792.
14 P. Aisen, M. Resnick and E. A. Leibold, *Curr. Opin. Chem. Biol.*, 1999, **3**, 200–206.
15 R. S. Eisenstein, *Annu. Rev. Nutr.*, 2000, **20**, 627–662.
16 T. A. Rouault, *Nat. Chem. Biol.*, 2006, **2**, 406–414.
17 C. Brugnara, *Clin. Chem.*, 2003, **49**, 1573–1578.
18 S. Lunvongsa, M. Oshima and S. Motomizu, *Talanta*, 2006, **68**, 969–973.
19 D. C. Gomes, M. A. Segundo, J. C. Lima and A. S. Rangel, *Talanta*, 2005, **66**, 703–711.
20 A. R. Timerbaev, E. Dabek-Zlotorzynska and A. G. T. Marc van den Hoop, *Analyst*, 1999, **124**, 811–826.
21 P. Vanloot, B. Coulomb, C. Brach-Papa, M. Sergent and J. L. Boudenne, *Chemosphere*, 2007, **69**, 1351–1360.
22 T. Shamspur, I. Sheikhshoaie and M. H. Mashhadizadeh, *J. Anal. At. Spectrom.*, 2005, **20**, 476–478.
23 L. Hu, Y. F. Zhang, L. Nie, C. G. Xie and Z. Q. Yan, *Spectrochim. Acta, Part A*, 2013, **104**, 87–91.
24 Z. Q. Yan, S. Y. Guang, H. Y. Xu and X. Y. Liu, *Analyst*, 2011, **136**, 1916–1921.
25 D. B. Wei, Y. L. Sun, J. X. Yu, G. H. Wei and Y. G. Du, *Sens. Actuators, B*, 2011, **160**, 1316–1321.
26 L. Hu, L. Nie, G. N. Xu, H. Shi, X. Q. Xu, X. Z. Zhang and Z. Q. Yan, *RSC Adv.*, 2014, **4**, 19370–719374.
27 A. Singh, S. Sinha, R. Kaur, N. Kaur and N. Singh, *Sens. Actuators, B*, 2014, **204**, 617–621.
28 Y. W. Ma, T. H. Leng, Y. R. Qu, C. Y. Wang, Y. J. Shen and W. H. Zhu, *Tetrahedron*, 2017, **73**, 14–20.
29 L. Qiu, C. C. Zhu, H. C. Chen, H. C. Chen, M. Hu, W. J. He and Z. J. Guo, *Chem. Commun.*, 2014, **50**, 4631–4634.
30 T. Nandhini, P. Kaleeswaran and K. Pitchumani, *Sens. Actuators, B*, 2016, **230**, 199–205.
31 N. R. Chereddy, K. Suman, P. S. Korrapati, S. Thennarasu and A. B. Mandal, *Dyes Pigm.*, 2012, **95**, 606–613.
32 H. Kim, B. A. Rao, J. Jeong, S. Angupillai, J. S. Choi, J. O. Nam, C. S. Lee and Y. A. Son, *Sens. Actuators, B*, 2016, **224**, 404–412.
33 Y. Xiang and A. J. Tiong, *Org. Lett.*, 2006, **8**, 1549–1552.
34 L. Dong, C. Xu, X. Zeng, L. Mu, S. F. Xue, Z. Tao and J. X. Zhang, *Sens. Actuators, B*, 2010, **145**, 433–437.
35 J. Mao, L. N. Wang, W. Dou, X. L. Tang, Y. Yan and W. S. Liu, *Org. Lett.*, 2007, **9**, 4567–4570.
36 N. V. Ghule, R. S. Bhosale, A. L. Bhosale, S. V. Bhosale and S. V. Bhosale, *Sens. Actuators, B*, 2016, **227**, 17–23.
37 P. Kaur and D. Sareen, *Dyes Pigm.*, 2011, **88**, 296–300.
38 T. B. Wei, P. Zhang, B. B. Shi, P. Chen, Q. Lin, J. Liu and Y. M. Zhang, *Dyes Pigm.*, 2013, **97**, 297–302.

39 T. Inoue, S. S. Pandy, N. Fujikawa, Y. Yamaguchi and S. Hayase, *J. Photochem. Photobiol., A*, 2010, **213**, 23–29.
40 T. Maeda, H. Nakao, H. Kito, H. Ichinose, S. Yagi and H. Nakazumi, *Dyes Pigm.*, 2011, **90**, 275–283.
41 Y. Wang, C. Wang, S. Xue, Q. Liang, Z. Li and S. Xu, *RSC Adv.*, 2016, **6**, 6540–6550.
42 H. J. Zhu, Y. H. Lin, G. M. Wang, Y. Q. Chen, X. H. Lin and N. Y. Fu, *Sens. Actuators, B*, 2014, **198**, 1201–1209.
43 B. H. Li, W. W. Li, Y. Q. Xu, J. Li, J. Tang and S. Sun, *Chem. Commun.*, 2015, **51**, 14652–14655.
44 Y. Xu, Z. Li, A. Malkovskiy, S. Sun and Y. Pang, *J. Phys. Chem.*, 2010, **114**, 8574–8580.
45 J. J. McEwen and K. J. Wallace, *Chem. Commun.*, 2009, **42**, 6339–6351.
46 Y. Xu, B. Li, L. Li, J. Xiao, S. Ouyang, Y. Sun and A. Pang, *Chem. Commun.*, 2014, **50**, 8677–8680.
47 H. Zheng, X. J. Zhang, X. Cai, Q. N. Bian, M. Yan, G. H. Wu, X. W. Lai and Y. B. Jiang, *Org. Lett.*, 2012, **14**, 1986–1989.
48 US EPA, *Secondary drinking water standards: guidance for nuisance chemicals n.d*.
49 S. Devaraj, Y. K. Tsui, C. Y. Chiang and Y. P. Yen, *Spectrochim. Acta, Part A*, 2012, **96**, 594–599.
50 E. Bozkurt, M. Arik and Y. Onganer, *Sens. Actuators, B*, 2015, **221**, 136–147.
51 M. J. Frisch, G. W. Trucks, H. B. Schlegel, G. E. Scuseria, M. A. Robb, J. R. Cheeseman, G. Scalmani, V. Barone, B. Mennucci, G. A. Petersson, H. Nakatsuji, M. Caricato, X. Li, H. P. Hratchian, A. F. Izmaylov, J. Bloino, G. Zheng, J. L. Sonnenberg, M. Hada, M. Ehara, K. Toyota, R. Fukuda, J. Hasegawa, M. Ishida, T. Nakajima, Y. Honda, O. Kitao, H. Nakai, T. Vreven, J. A. Montgomery Jr, J. E. Peralta, F. Ogliaro, M. Bearpark, J. J. Heyd, E. Brothers, K. N. Kudin, V. N. Staroverov, R. Kobayashi, J. Normand, K. Raghavachari, A. Rendell, J. C. Burant, S. S. Iyengar, J. Tomasi, M. Cossi, N. Rega, J. M. Millam, M. Klene, J. E. Knox, J. B. Cross, V. Bakken, C. Adamo, J. Jaramillo, R. Gomperts, R. E. Stratmann, O. Yazyev, A. J. Austin, R. Cammi, C. Pomelli, J. W. Ochterski, R. L. Martin, K. Morokuma, V. G. Zakrzewski, G. A. Voth, P. Salvador, J. J. Dannenberg, S. Dapprich, A. D. Daniels, O. Farkas, J. B. Foresman, J. V. Ortiz, J. Cioslowski and D. J. Fox, *Gaussian 09, revision D.01*Gaussian, Inc., Wallingford, CT, 2013.